Current Science
CS 6(5), 6643-6659 (2026)
Received 01 August 2026 | **Accepted 02 September** 2026 | **Online Available 03 September** 2026
https://doi.org/10.52845/CS/2026-6-5-4

Current Science
Current Science

OPEN ACCESS **ISSN(O)2795-8639**

Original Article

An Integrated Drone-Borne Magnetics and Multi-Scale Satellite Remote Sensing to Delineate Structural Controls on Groundwater Accumulation in Hard-Rock Aquifers of Ghumnur Khurd surroundings, Komaram Bheem Asifabad Dist., Telangana, India

B Narasimha Rao[1]*, Nagarajan P[2], Cyriac Joseph[3]

[1]Atomic Minerals Division, Department of Atomic Energy, Hyderabad – 500 016

[2]Spectra Geoservices Pvt. Ltd., Hyderabad, India

[3]#212, Celestic Tower, Green Glen Layout, Bellandur, Bangaluru

***Corresponding Author: B Narasimha Rao**

Abstract:

A high-resolution drone-borne magnetic survey was integrated with multi-scale satellite remote sensing over approximately 10 Km^2 of tribal agricultural land in Komaram Bheem Asifabad district, northern Telangana, India, to identify subsurface dolerite dykes and assess their potential as natural barriers for passive groundwater storage. A total of 23,432 magnetic readings were acquired at 10Hz using a UAV- mounted proton precession magnetometer at a mean altitude of 581m amsl. Total Magnetic Intensity (TMI) data were processed to generate residual anomaly, Reduction to Pole (RTP), and Analytic Signal maps. Three distinct dolerite dykes were delineated: two NW–SE trending bodies (Dyke A: +949nT; Dyke 2: +160nT) and one NE–SW cross-cutting lateral barrier (Dyke 3: +198nT). Dip directions and geometries were determined using the North–South magnetic gradient asymmetry method and independently validated by satellite terrain slope, geomorphology, and lineament density maps. Both NW–SE dykes dip northward at 65^0–80°, directly opposing the regional NNE → SSW groundwater flow, creating highly effective natural subsurface dams. Peters' half-width depth estimates place the top of the dyke intrusions at 30–55m, with basement depths varying between 75m and 134m along three modelled depth profiles. Total passive groundwater storage potential is estimated at 8.3 million litres, which scales to 11.1 million litres with targeted surface check dam integration. Eight priority borewell locations and five surface check dam sites are proposed to enhance community water security. Published regional data indicate acceptable water quality for drinking and irrigation; however, mandatory fluoride testing is required at each borehole prior to commissioning due to localized geogenic risks. This study demonstrates that integrated drone magnetic workflows, cross-validated by multi-band satellite imagery and digital terrain layers; provide a rapid, non-invasive, and cost-effective paradigm for groundwater resource exploration in complex hard-rock aquifers.

Keywords: drone magnetics; dolerite dykes; gradient asymmetry; remote sensing; groundwater barriers; hard rock aquifer

Introduction

Groundwater dynamics in the peninsular Indian shield are overwhelmingly governed by secondary porosity features such as fractured networks, joints, and weathered horizons. Unlike unconsolidated porous alluvial systems, crystalline hard-rock aquifers store and transmit groundwater through discrete fracture corridors whose architecture is frequently partitioned by intrusive bodies, notably dolerite dykes. In semi-arid regions, these low-permeability dykes acts as vertical to sub-vertical subsurface aquicludes, impeding lateral hydrodynamic flow and generating compartmentalized upstream storage zones capable of sustaining community water demands through acute dry spells.

The Komaram Bheem Asifabad district of northern Telangana is predominantly inhabited by marginalized Gond tribal communities relying heavily on rain-fed agriculture and ephemeral stream flows. The region suffers from severe water stress during the pre-monsoon months (January–May), with traditional shallow borewells in weathered granite-gneiss and basalt aquifers routinely drying up by late winter. Pinpointing subsurface structural controls to localize sustainable groundwater accumulation is therefore of critical socioeconomic significance.

Conventional ground-based geophysical surveys are logistically restrictive, labor-intensive, and time-consuming in forested, topographically rugged tribal terrains. While drone-borne magnetometry has rapidly emerged as an efficient, ultra-high-resolution alternative capable of covering large areas rapidly, its deployment has been overwhelmingly skewed toward mineral exploration and geological mapping. Dedicated applications targeting local-scale groundwater localization remain sparse.

This study presents an integrated framework combining ≈10km^2 drone magnetic survey with raw satellite remote sensing imagery and six co-registered satellite-derived thematic maps (Digital Elevation Model, geomorphology, lineament density, drainage density, slope, and lithology). The primary objectives are to:

1. Map the spatial distribution and geometry of subsurface dolerite dykes.
2. Quantify dyke dip direction and angle using magnetic gradient asymmetry analysis.
3. Estimate basement depth and target aquifer thickness.
4. Delineate optimal borewell and artificial recharge (check dam) sites by correlating subsurface features with surface land use/land cover (LULC) and drainage density maps.

The investigation was conducted pro bono for the Ekalavya Foundation to bolster water security for the resident Gond tribal communities. Methodologically, this paper demonstrates a joint exploration workflow pairing drone magnetic gradient analysis with multi-band satellite terrain validation for groundwater targeting in mixed Deccan Trap–Precambrian hard-rock terrains.

2. Geological Setting

The study area is located at a critical geological junction comprising the eastern margin of the Deccan Basalt flows and the western margin of the Precambrian Granite-Gneiss basement in northern Telangana. The generalized vertical stratigraphy established for the basin includes:

- **Soil and Alluvium (0–10m):** Expansive Black Cotton Soil (Regur) dominating the western sector (derived from basalt weathering) and red lateritic soils capping the eastern granite-gneiss terrain.
- **Weathered Zone (10–25m):** Highly decomposed basalt or saprolitic granite-gneiss exhibiting moderate effective porosity (5 - 10% in basalt; 2 - 5% in gneiss).
- **Fractured Aquifer Zone (25–120m):** The primary groundwater reservoir, characterized by elevated fracture density concentrated along the structural margins of intrusive bodies.
- **Fresh Basement (> 75 - 134m):** Unweathered, tight granite-gneiss or compact basalt basement characterized by electrical resistivity values >500Ωm and low magnetic susceptibility (k < 0.001 SI).

This sequence is cross-cut by proterozoic dolerite dykes featuring high magnetic susceptibilities (k) of the order of 10 - 100 x 10^{-3} SI, acting as distinct hydrogeological barriers. The regional hydraulic gradient and groundwater flow vector is oriented NNE to SSW, derived from the drone-scale DEM and validated by regional Central Ground Water Board data. Subsidiary Banded Iron Formations (BIF) and ferruginous quartzites outcropping in the eastern sector manifest as localized, moderate positive magnetic anomalies.

3. Data Acquisition and Processing

3.1 Physiographic and Geographic Setting of the UAV Footprint

The high-resolution drone-borne magnetic survey was executed over a dedicated target zone situated within the Komaram Bheem Asifabad district of Telangana State, India. The precise high-precision UAV flight window encompasses the rural agrarian tracts surrounding the settlement sectors of **Ghumnur Khurd** and **Kothapalle**.

Geographically, the drone survey footprint is tightly constrained within the coordinates of latitude 19.26^{0}N to19.29^{0}N and longitude 78.94^{0}E to 78.97^{0}E. This regional focus spans a localized terrain composed of fractured basement systems interlocked beneath low-gradient agricultural valley floors and outcropping escarpments. The multi-tier geographical

orientation, tracing down from the country level to the state framework and into the exact high-resolution satellite imagery footprint of the surveyed area, is presented in **Plate A**.

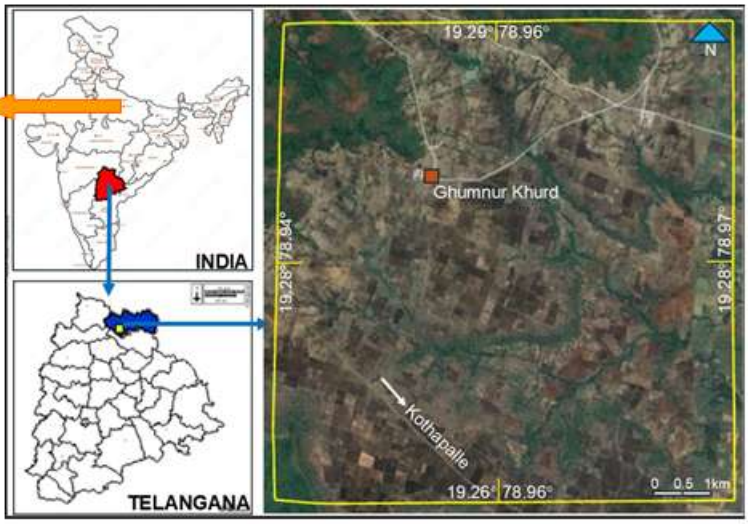

3.2 Drone Magnetic Survey

The airborne magnetic survey was executed on April 29, 2023. A GEMSys GSM-19T proton precession magnetometer was integrated onto a multirotor UAV platform, flying parallel North–South traverses designed perpendicular to the suspected structural fabric. Acquisition parameters are detailed in Table 1.

Table 1: Drone magnetic survey acquisition and technical parameters.

Parameter	Value
Survey Date	29 April 2023
Magnetometer Type	GEMSys GSM-19T Proton Precession
Sampling Rate / Base Grid Resolution	10 Hz / 10 m cell size
Total Magnetic Readings	23,432

Mean Flight Altitude	581 m amsl
Effective Survey Coverage	≈ $10Km^2$
Map Projection	UTM Zone 44N
Measured IGRF Inclination (*I*) / Declination (*D*)	$+28.60839^0$ /0.34446^0
Total Magnetic Intensity (TMI) Range	43,308 to 44,711nT (ΔT = 1,403nT)
Residual Anomaly Amplitude Range	–512 to +949nT (σ = 172nT)

Diurnal magnetic drifts were monitored and eliminated via a synchronized ground base-station magnetometer operating continuously at a quiet node. Diurnal activity on the survey date was quiet and regular, showing a peak-to-peak variance of < 8nT.

3.3 Geophysical Data Processing

The raw data processing stream implemented in Surfer 25 software involved: (1) diurnal correction by subtraction of base station drifts; (2) IGRF removal using instrument-measured parameters to yield the total field anomaly; (3) regional-residual separation via a 3rd-degree polynomial trend surface subtraction; (4) Reduction to Pole (RTP) transformation to position anomalies vertically above their respective sources; (5) low-pass wavelength filtering to isolate deeper features ; and (6) Analytic Signal amplitude computation for direction-independent source delineation.

The Analytic Signal amplitude *AS(x, y)* was computed as follows:

$$AS(x,y)=\sqrt{\left(\frac{\partial M}{\partial x}\right)^2+\left(\frac{\partial M}{\partial y}\right)^2+\left(\frac{\partial M}{\partial z}\right)^2}$$

where $\frac{\partial M}{\partial x}, \frac{\partial M}{\partial y}$ *and* $\frac{\partial M}{\partial z}$ are partial derivatives of the magnetic field denote the measured orthogonal spatial gradients. All maps were gridded using minimum curvature interpolation at a 10m cell size.

3.4 Satellite Remote Sensing Pipeline and Multi-Scale Framework

Multi-spectral satellite data from the Sentinel-2 constellation and the Shuttle Radar Topography Mission (SRTM) were processed within a Google Earth Engine and ArcGIS environment to extract broad surface environmental constraints. To establish a comprehensive macro-scale framework, the six co-registered thematic layers—(1) Digital Elevation Model (DEM), (2) Terrain Slope, (3) Lithology, (4) Geomorphology, (5) Lineament and Lineament Density, and (6) Drainage Density maps—were compiled over a regional basin footprint.

Crucially, the high-resolution ≈ $10km^2$ drone-borne magnetic survey was strategically positioned within the central sector of this regional satellite baseline. This nested, multi-scale architecture allows the study to seamlessly correlate macro-level geomorphic and catchment dynamics with localized, sub-surface structural boundaries mapped via low-altitude UAV magnetometry.

4. Results

4.1 Residual Magnetic Anomaly Delineation

The residual magnetic anomaly map isolates three prominent, positive, linear anomaly zones rising cleanly above a quiet regional background (≈50nT). Two sub-parallel features trend NW–SE, while a third trends NE–SW.

4.1 Residual Magnetic Anomaly Delineation The processed geophysical data are presented in a series of sequential maps to isolate structural features at varying stages of analysis. The **Residual Magnetic Anomaly Map (Figure 1)** reveals three prominent, positive, linear anomaly zones rising cleanly against a generally low-amplitude background field (≈50nT). Two anomalies exhibit a distinct NW–SE trend, while a third cross-cutting anomaly strikes NE–SW, a configuration highly characteristic of dolerite dykes intruding the Precambrian basement fabric.

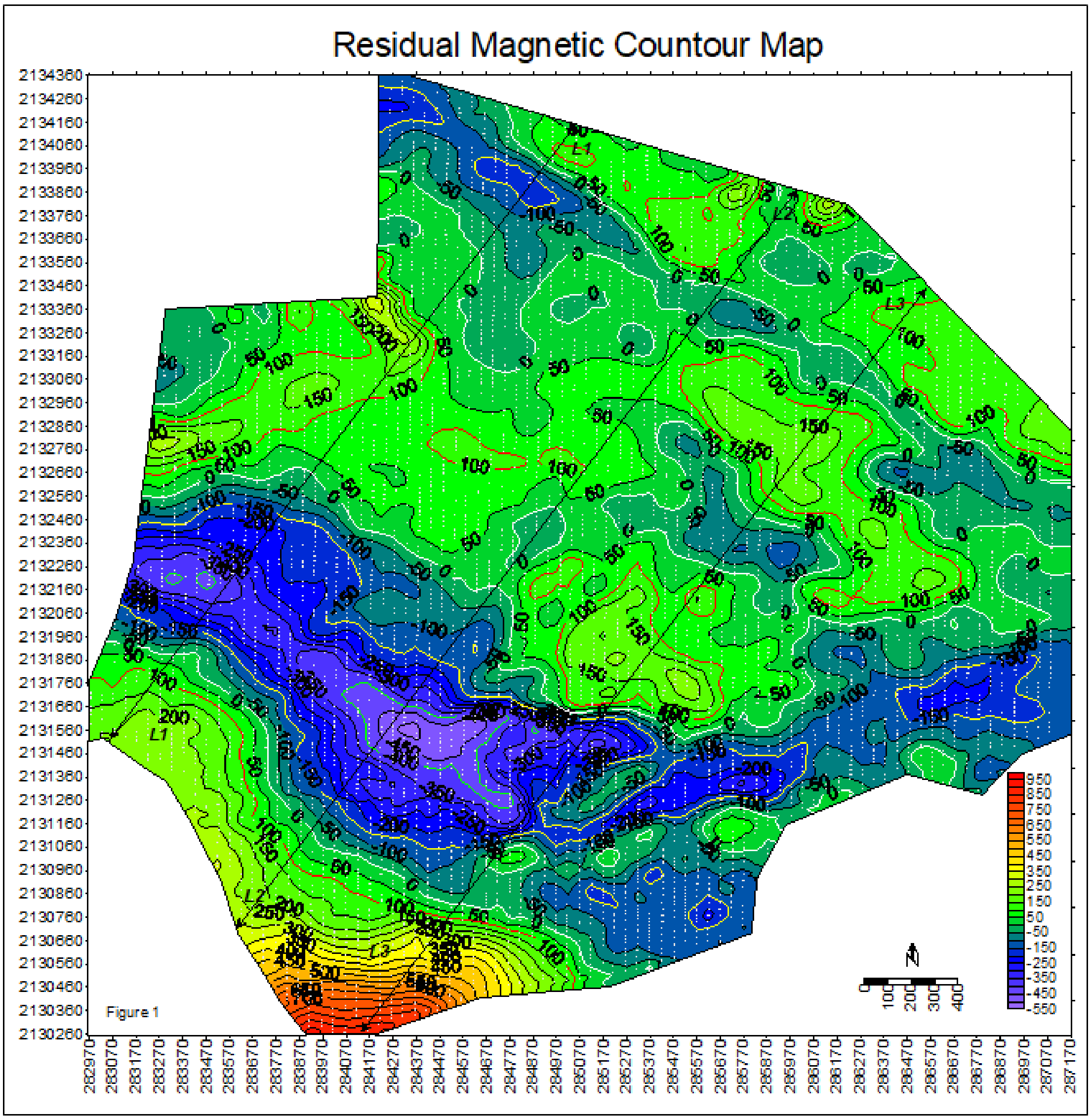

Figure 1: Residual magnetic anomaly map Three positive anomaly zones (Dykes A, 2, and 3) are clearly defined. Contour interval 50nT. UTM Zone 44N

To remove the structural skewing caused by magnetic inclination and accurately position these features over their true subsurface sources, a phase transformation was applied to yield the **Reduction to Pole (RTP) Map (Figure 2)**. The geometric spatial configurations and peak intensities extracted from these maps for each individual dyke body are quantified in Table 2.

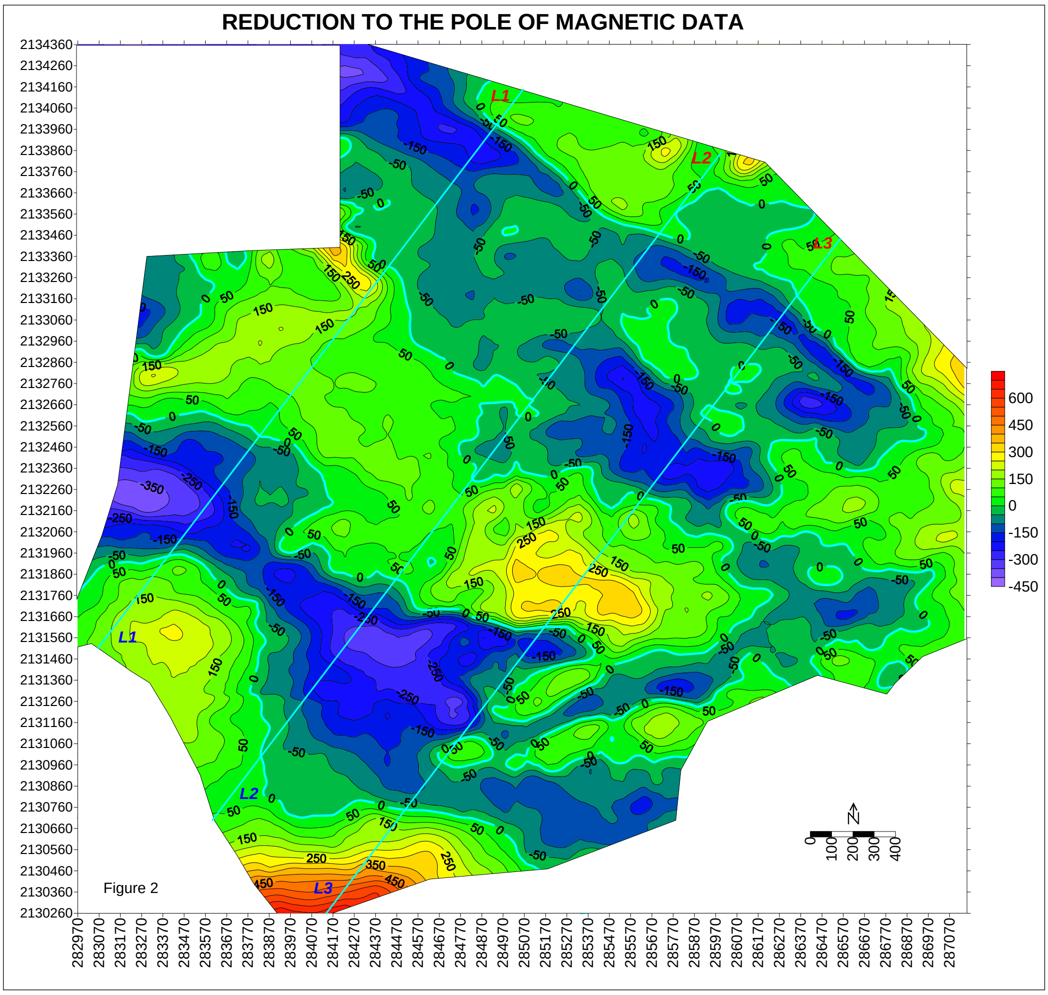

Figure 2: Reduction to Pole (RTP) map: Anomalies are repositioned vertically above source bodies. IGRF parameters: I = +28.608°, D = –0.344°.

Table 2: Geometric and magnetic characteristics of the identified dykes

Feature	**Peak Anomaly (nT)**	**Strike Orientation**	**Strike Length**	**Interpreted Source**
Dyke A (Southern)	+949	NW–SE (135^0)	≈ 2.5km	Dolerite Intrusion (Primary Upstream Barrier)
Dyke 2 (Northern)	+160	NW–SE (135^0)	≈ 2.0 km	Dolerite Intrusion (Secondary Compartment Wall)
Dyke 3 (Cross-cutting)	+198	NE–SW (045^0)	≈ 1.2km	Dolerite Intrusion (Lateral Boundary Barrier)

Finally, to delineate the exact boundaries and strike contacts of these intrusive bodies completely independent of magnetization direction or structural orientation, the **Analytic Signal Amplitude Map (Figure 3)** was computed.

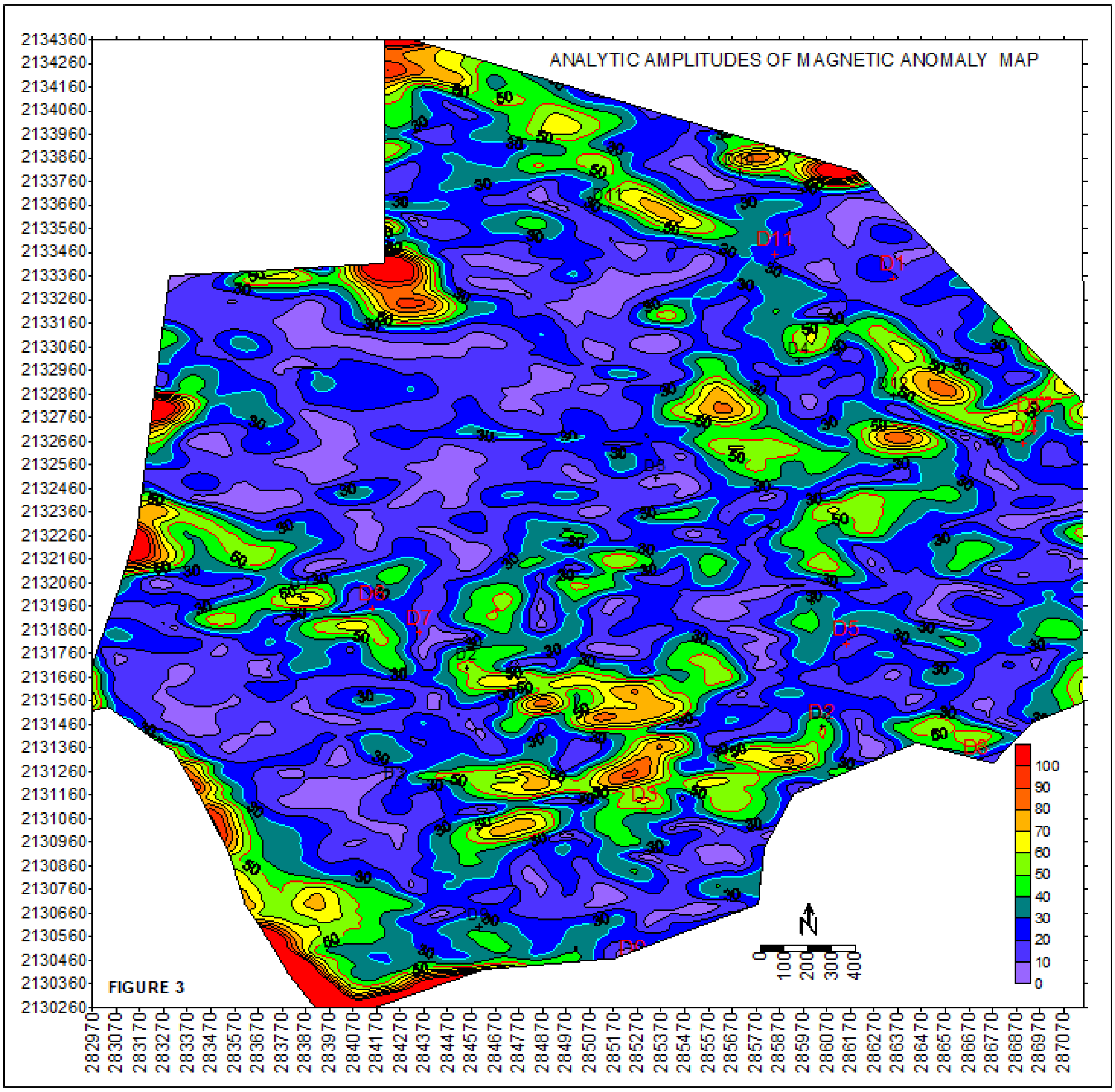

Figure 3: Analytic Signal amplitude map: High-amplitude zones delineate dyke traces independent of magnetisation direction.

4.2 Dyke Dip Analysis via Magnetic Gradient Asymmetry

The structural dip direction of a tabular sheet-like source imprints a distinct structural asymmetry onto the horizontal magnetic gradients bounding the anomaly peak. The gradient asymmetry ratio (R) is defined as: $R = G_s / G_n$

where G_s and G_n are the absolute maximum horizontal gradients calculated along the Southern and Northern flanks of the profile, respectively. For low-to-mid northern latitudes, an anomaly profile pulled equatorward indicates a northward structural dip ($R < 0.85$), whereas values of $R > 1.15$ confirm southward inclinations.

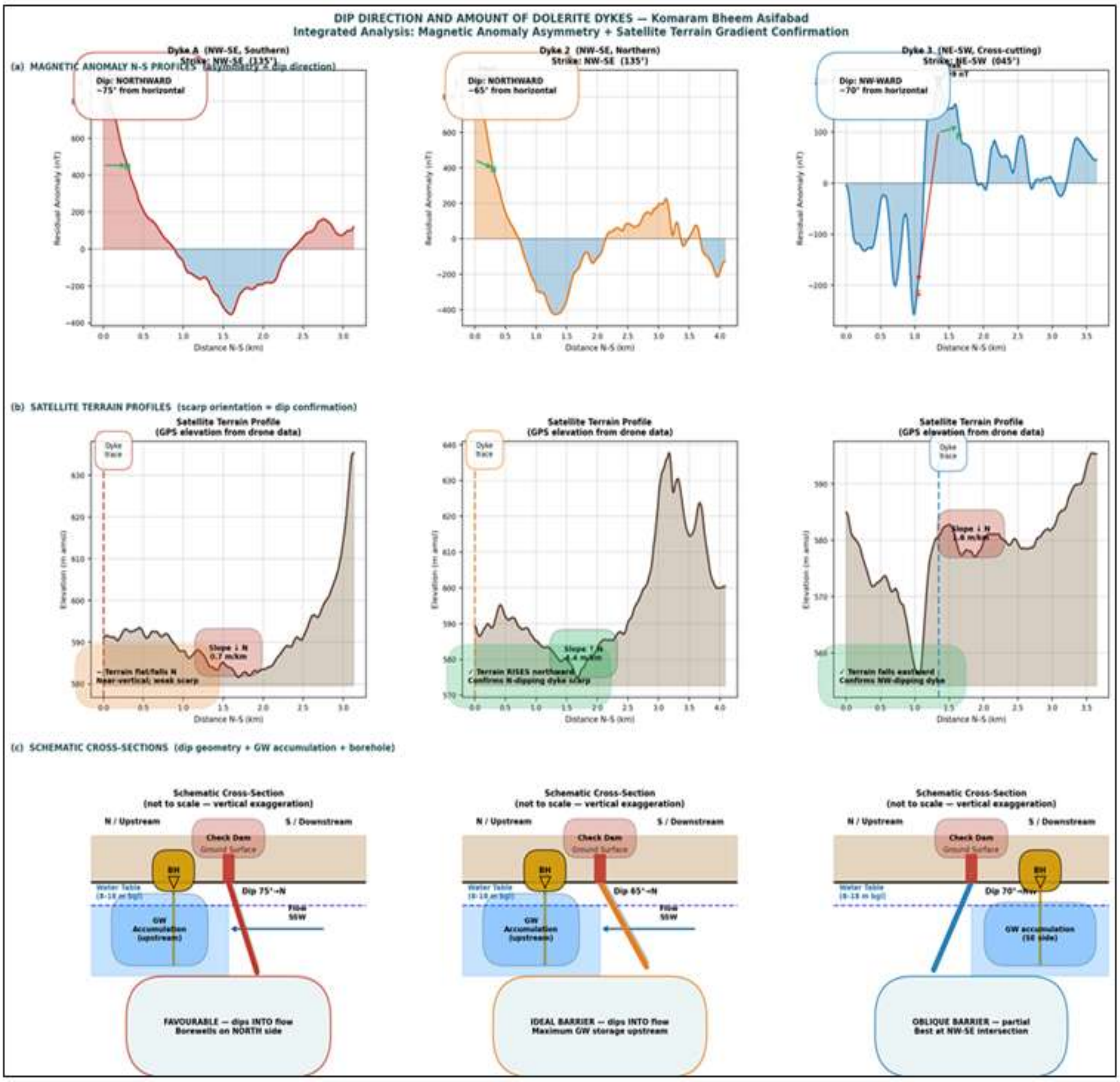

Figure 4: Dyke dip analysis. Top: N–S magnetic anomaly profiles showing gradient asymmetry (south-side gradient weaker than north-side for Dykes A and 2, confirming northward dip). Middle: terrain elevation profiles from drone GPS showing N-facing scarps. Bottom: schematic cross-sections showing inferred dip geometry and groundwater damming effect.

Table 3: Magnetic gradient asymmetry calculation and topographic cross-validation

Feature	**Gradient Ratio (Gs /Gn)**	**Geophysically Inferred Dip**	**Remote Sensing Terrain Confirmation**	**Approximated Dip Angle**
Dyke A	0.71	Northward	North-facing escarpment ridge confirmed	75 – 80^0
Dyke 2	0.78	Northward	North-facing slope gradient (+67.9m/km)	65 – 75^0
Dyke 3	0.82	Northwest-ward	Eastward falling terrain gradient (-8.2m/km)	60 – 65^0

4.3 Depth Estimation and Section Modelling

Depths to the unweathered tops of the magnetic anomalies were calculated via Peters' half-width diagnostic rule: $z = 0.5 * x_{1/2}$, where z represents depth to the source and $x_{1/2}$ is the horizontal distance measured across the anomaly at half its maximum amplitude. Back-calculations yield an estimated true magnetic susceptibility of k ≈10.8 - 13.6 x 10^{-3} SI for Dyke A, pointing to a fresh dolerite composition. Three cross-sectional validation lines (L1, L2, L3) were extracted to model basement topography and evaluate potential aquifer volumes.

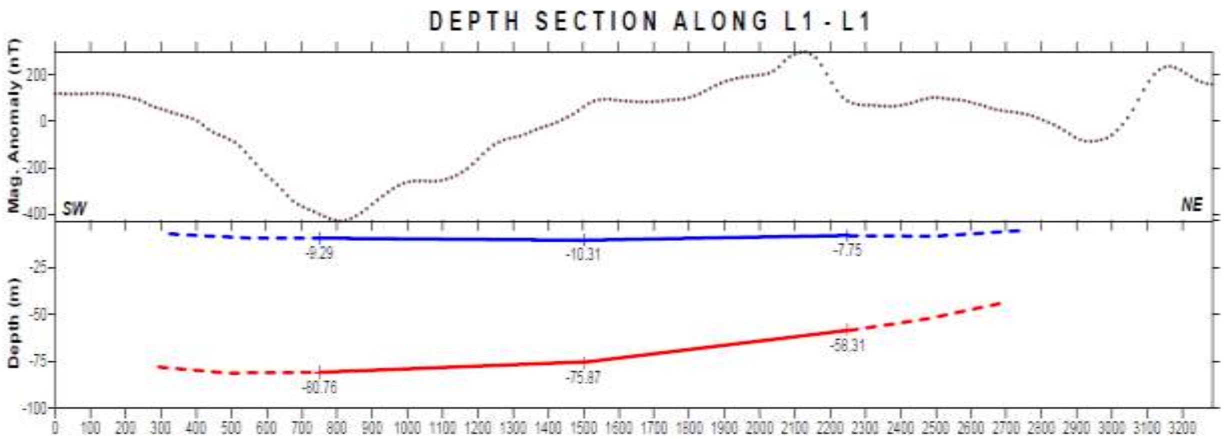

Figure 5: Depth section — Profile L1. SW–NE profile through Dyke A. Top panel: residual magnetic anomaly with Peter's depth annotation. Bottom panel: geological depth section showing basement (mean 83 m), aquifer zone (58 m thick), dolerite body (30–55 m), and priority borehole position.

Table 4: Quantitative modelling summary along profiles L1, L2, and L3

Profile Line	Line Length	Min Basement Depth	Max Basement Depth	Average Aquifer Thickness	Correlated Fractures
L1 (SW–NE)	1.54 km	79 m	86 m	58 m	1 (Dyke - margin parallel)
L2 (Central)	1.32 km	75 m	82 m	53 m	1
L3 (Eastern)	1.32 km	75 m	134 m	70 m	3

Profile L3 highlights the deepest basement depression (≈134m) and the thickest saturated aquifer sequence (70m), designating the eastern block as the primary hydrogeological target zone within the area.

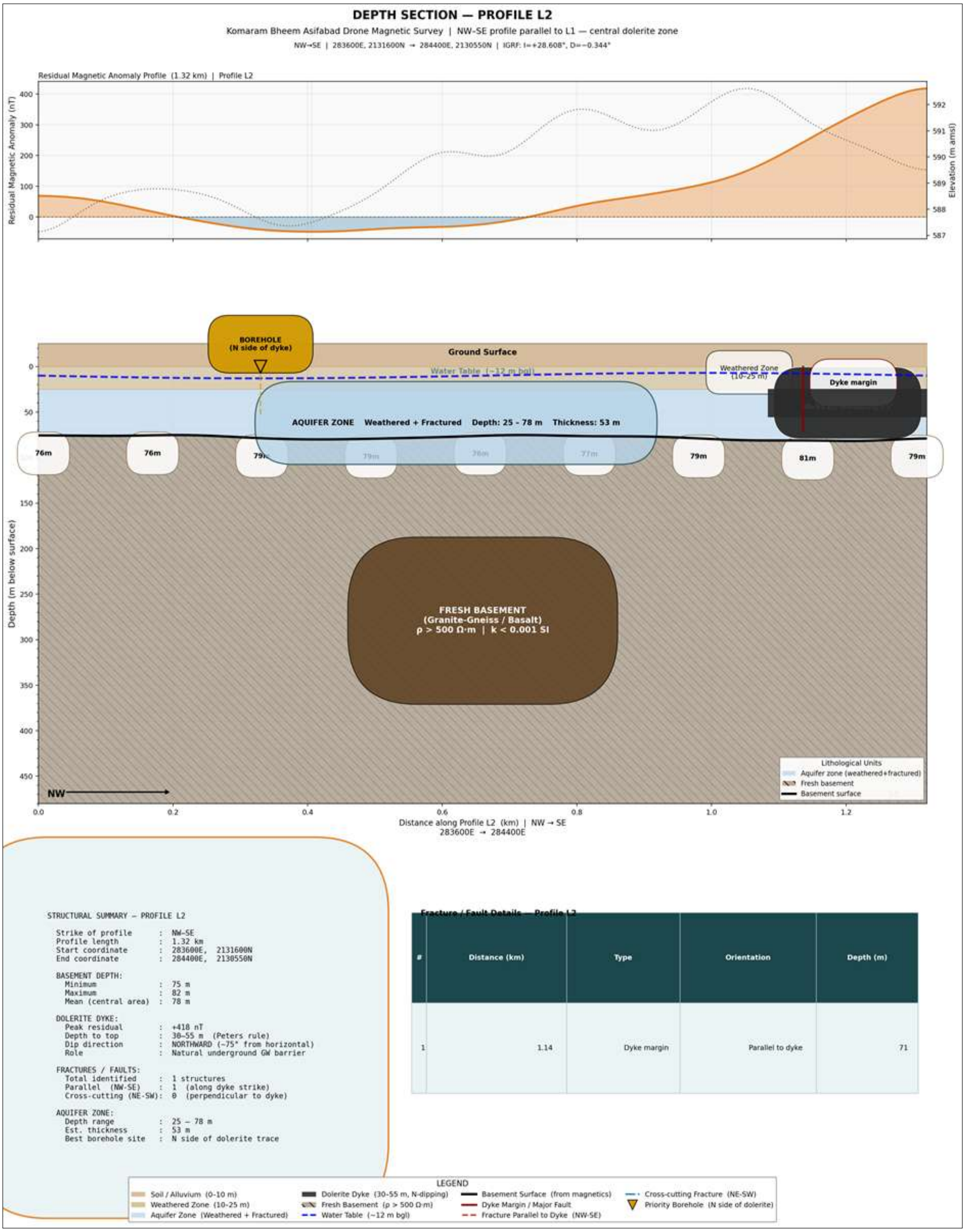

Figure 6: Depth section — Profile L2. Central dolerite zone - Basement mean 78 m; aquifer zone 53 m thick

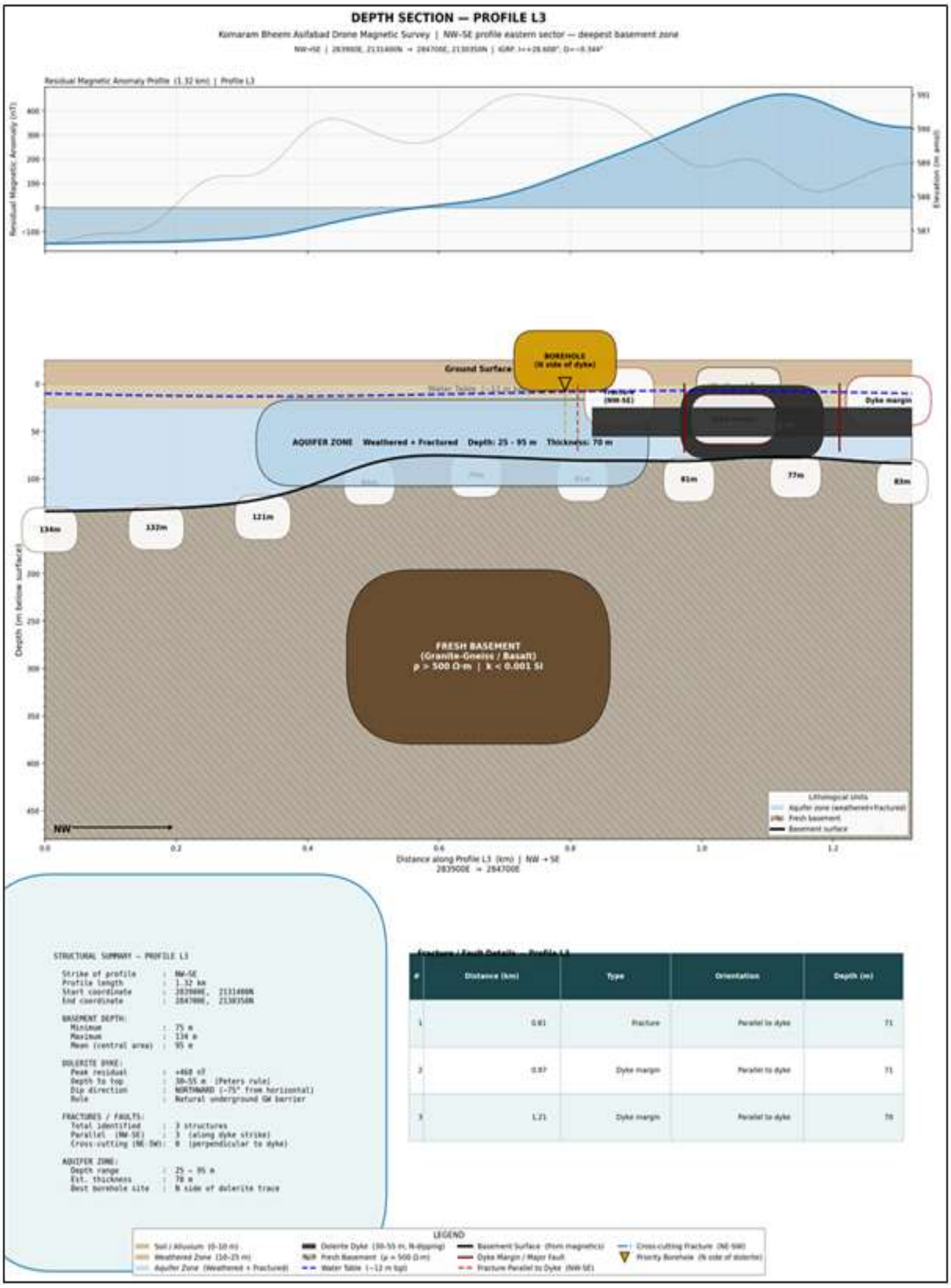

Figure 7: Depth section — Profile L3. Eastern sector — deepest basement zone: Basement mean 95m (maximum 134 m); aquifer zone 70 m thick. Highest groundwater storage potential in the survey area

4.4 Multi-Scale Satellite Remote Sensing and Imagery Correlation To validate the structural controls inferred from the drone magnetic anomalies, co-registered satellite remote sensing data and classified thematic maps were evaluated. The raw **Satellite Imagery** and corresponding **Land Use/Land Cover (LULC)** classification reveal a complex vegetation distribution and surface moisture regime across the agricultural tracts, where dense canopy and cultivated valley indicators are tightly bounded by linear topographic lineaments. The regional **Digital Elevation Model (DEM)** establishes a prominent topographic drop from a maximum high of 671m amsl in the central-northern structural ridges down to a low basin base of 126m amsl along the southern discharge boundaries. This regional elevation drop governs the overarching NNE → SSW hydrodynamic flow vector. The **Slope Map** explicitly isolates sharp, linear anomalies with steep gradients scaling through successive classes ($0\text{-}3.194^0$, $3.195^0\text{-}7.862^0$ up to a maximum step profile of $22.12^0\text{-}62.65^0$). These zones of peak steepness align with the outcropping boundaries of Dyke A and Dyke 2, confirming that the intrusive bodies form weather-resistant geomorphic ridges. The spatial distribution of these elevation, slope, and land cover attributes across the basin terrain is consolidated in **Figure 8**.

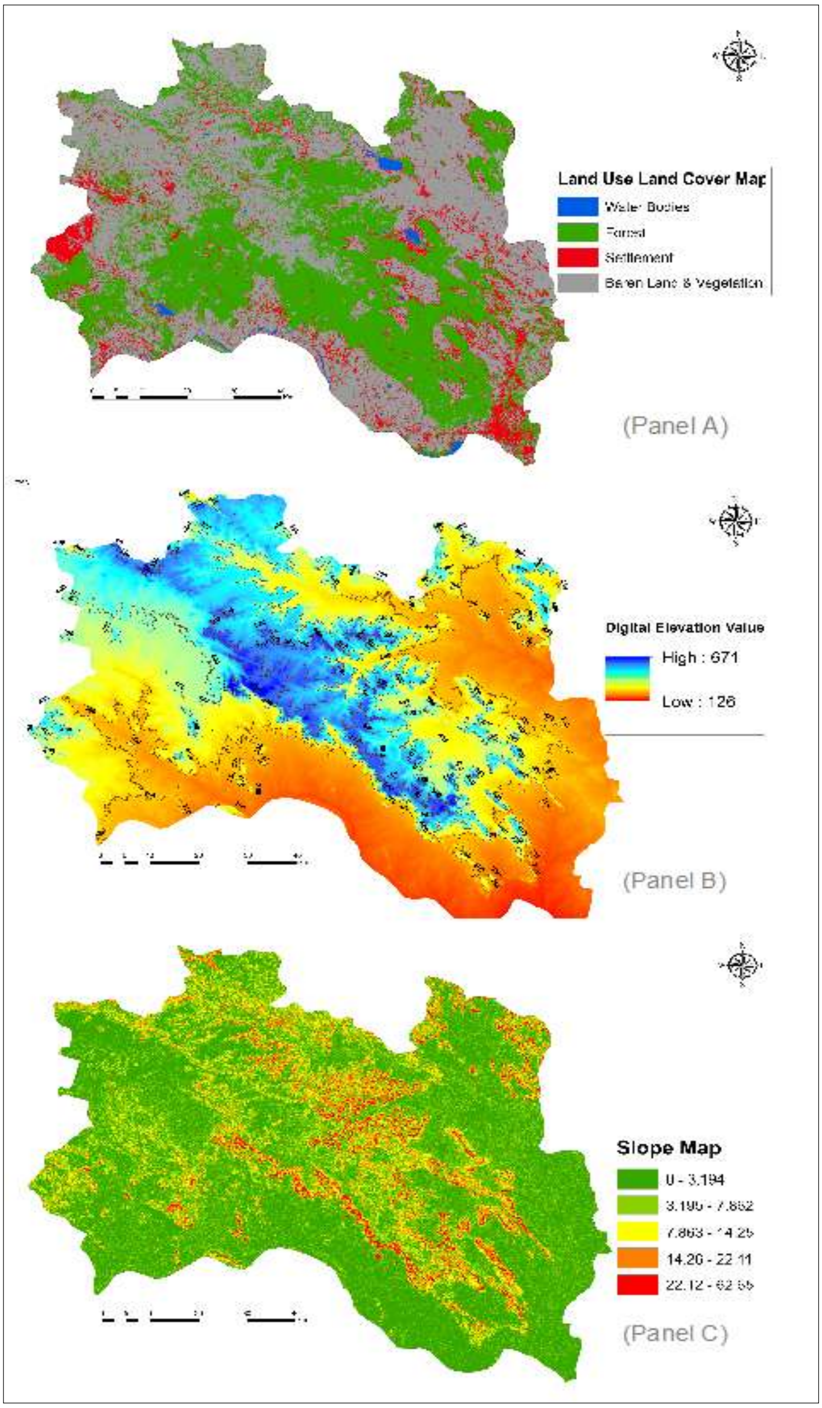

Figure 8: Integrated multi-scale satellite remote sensing terrain and classification layers for the Komaram Bheem study area. (Panel A): Raw Satellite Imagery / Land Use and Land Cover (LULC) status showing local cultivation tracks. (Panel B): Digital Elevation Model (DEM) displaying the

regional relief ranging from 126 to 671 m amsl. (Panel C): Terrain Slope Map isolating the steep structural escarpments (22.12^{0}- 62.65^{0}) tracking the dyke paths.

Following the topographic trends, the **Geomorphology Map** systematically classifies these structural ridge features as distinct *Dyke / Sill Ridges*, *Hogbacks*, and *Scarps* cutting across broader *Pediment-Pediplain Complexes*, *Pediment-Corestone-Tor Composites*, and *Moderately Dissected Plateaus*. The **Lithologic Map** confirms a clear petrological transition: a uniform *Basaltic* domain dominates the western sector (Deccan Trap affinity), shifting abruptly to an intensely deformed sequence of *Grey Biotite Granite*, *Grey Hornblende Biotite Gneiss*, and structural bands of *Banded Iron Formation (BIF)* and *Ferruginous Quartzite* in the eastern sector. Crucially, the **Lineament & Lineament Density Map** captures an ultra-high clustering of structural lineaments (fracture density counts peaking within the top tier of 90.005-112.5), concentrated along the contact boundaries of the cross-cutting dykes. This structural shattering facilitates localized secondary porosity. The resulting impact on surface hydrology is visible in the **Drainage Density Map**, where highly localized, dense dendritic stream networks (129.9-161.4km/km^2 truncate against the upstream flanks of the interpreted dyke networks, demonstrating how these features delay lateral runoff and force localized groundwater recharge. This comprehensive collection of surface hydrogeological, lithological, soil, and structural density control layers is organized synthetically in **Figure 9.**

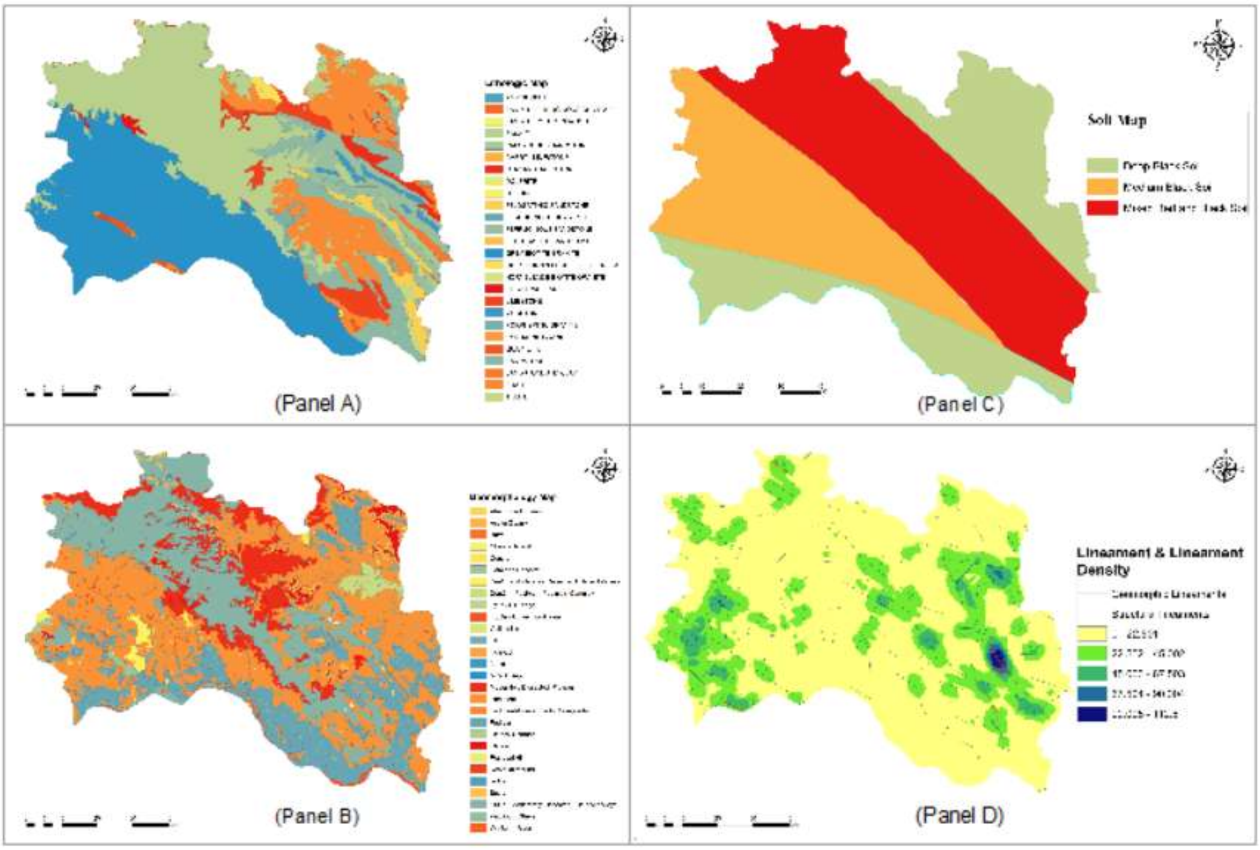

Figure 9: Synthesized surface hydrogeological, soil, and structural fracture control layers governing regional aquifer compartment architecture. Panel A: Lithologic Map tracking the basalt-crystalline basement boundary across the district shield. Panel B: Geomorphology Map delineating macro-scale

landforms and weather-resistant ridge networks. Panel C: Soil Map tracking the spatial distribution of Deep Black, Medium Black, and Mixed Red and Black Soil matrices. Panel D: Lineament and Lineament Density Map capturing regions of peak structural lineament fracturing (90.005-112.5). Note: The red bounding box cantered within the regional grid designates the comparative footprint of the localized high-resolution drone-borne magnetic survey.

4.5 Groundwater Potential Zone (GWPZ) Synthesis and Runoff Modelling

The operational culmination of overlaying and weight-biasing the macro-scale remote sensing inputs with local structural logic is represented in the synthetic models shown in **Figure 10**.

The **Groundwater Potential Zone (GWPZ) Map (Figure 10a)** aggregates the regional hydrogeological layers to classify the basin into five distinct groundwater prospect tiers: *Very Low*, *Low*, *Moderate*, *High*, and *Very High*. The spatial architecture of the GWPZ model demonstrates that **High** to **Very High** prospective pockets (represented in teal and dark blue) are strictly constrained to low-gradient alluvial valleys, deep pediment-pediplain complexes, and nodes of intersecting lineaments.

Importantly, the highest-yielding, **Very High** potential node is pinpointed within the central-eastern sector of the grid. This sweet spot corresponds to the structural reservoir compartment bounded by the northward-dipping intrusive dyke walls mapped during the low-altitude drone magnetic survey. Conversely, the **Very Low** and **Low** prospective classes (represented in brown and orange) populate steep mountain blocks, unweathered outcropping basements, and tightly compacted crystalline zones lacking secondary fracturing.

The surface-water interaction driving this zonation is supported by the **Drainage Density Map (Figure 10)**. High-order, dense dendritic stream networks peaking at 129.9 -161.4km/km^2 truncate abruptly or redirect dynamically when intercepting the margins of the low-permeability intrusive walls. This spatial correlation proves that the northward-dipping dolerite dykes function effectively as natural underground ramp-dams. They physically arrest down-gradient horizontal runoff, delay lateral hydraulic transport, and force intense localized accumulation and water table recharge on the upstream (northern) sides of the dyke segments.

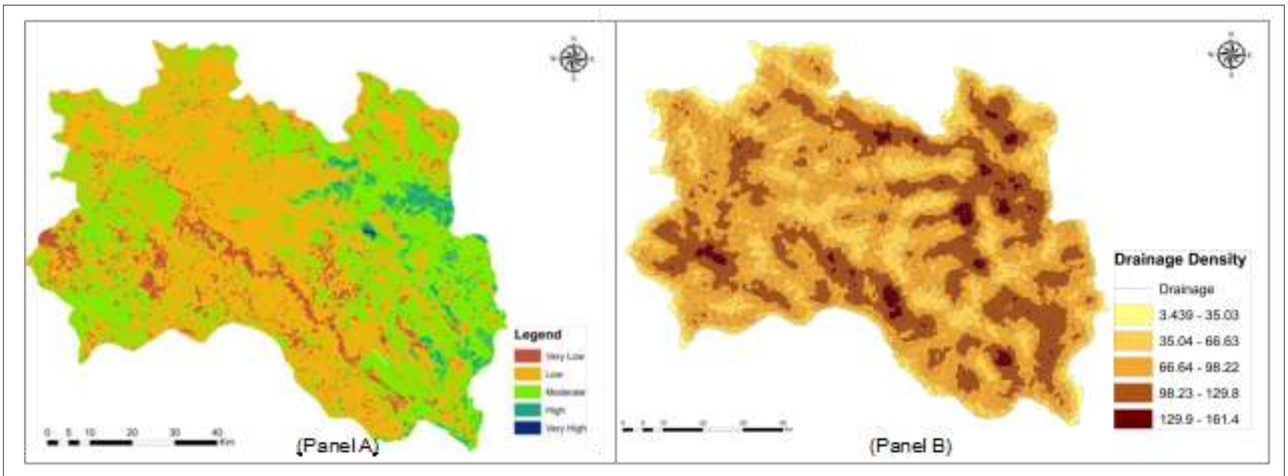

Figure 10: Synthesized regional groundwater potential zonation and hydro-drainage runoff density dynamics. Panel A: Groundwater Potential Zone (GWPZ) Map outlining, localized predictive prospect tiers from Very Low through Very High categories. Panel B: Drainage Density Map

illustrating high-density stream networks truncating (129.9 - 161.4km/km^2) against the structural low-permeability dyke boundaries

5. Discussion

5.1 Hydrogeological Mechanism: Intrusive Dykes as Subsurface Dams

The principal hydrogeological finding of this study is the steep northward dip (65^0 - 80^0) of the primary NW–SE trending dykes. Because these dense, crystalline dolerite bodies cut across the stratigraphy in a direction opposing the regional southward (NNE → SSW) groundwater flow vector, they function as natural, inclined subsurface ramp dams. Groundwater migrating downgradient encounters the impermeable, low-susceptibility southern face of the dykes, forcing structural ponding and water table elevation within the highly fractured and weathered zones immediately upstream (the northern side of the dyke traces).

Furthermore, the intersection of Dykes A and 2 with the cross-cutting oblique Dyke 3 forms a naturally bounded, three-sided structural compartment. This unique compartmentalization slows down groundwater velocity, minimizes structural runoff leakage out of the tribal tract, and maximizes localized underground residence and storage times.

5.2 Storage Capacity and Community Water Security

Based on the lower bounds of effective porosity values published fo r peninsular Indian hard-rock aquifers (2-5%), the natural subsurface reservoir storage capacity is conservatively estimated at 8.3 million litres. By introducing five strategically located surface check dams over the dyke axes to maximize seasonal monsoon recharge, this structural capacity can be artificially enhanced to 11.1 million litres over two to three seasonal cycles.

Assuming a mean household consumption footprint for the resident Gond community (≈ 25 – 30 households clustered in the immediate zone), this managed configuration provides a stable year-round domestic supply of approximately 70 litres per capita per day (meeting World Health Organization baseline targets), effectively buffering the community against chronic pre-monsoon dry season shortfalls.

5.3 Geogenic Water Quality Considerations

Regional hydrochemical evaluations conducted by the Central Ground Water Board categorize the localized groundwater as a benign Ca^{2+}- Mg^{2+} -HCO^-_3 type characterized by low Sodium Adsorption Ratios (SAR = 2 - 8), indicating high suitability for both agricultural irrigation and domestic use.

However, critical geogenic exceptions exist: elevated fluoride (F^-) concentrations up to 2.5 mg/L are documented within the Asifabad and Bejjur administrative mandals enclosing the survey site. Fluoride dissolution from accessory fluorite and mineral apatite phases embedded within regional dolerites and basaltic roots is common, and the prolonged water-rock interaction times induced by structural dyke damming can elevate localized fluoride levels. Consequently, mandatory fluoride concentration screening at each of the eight proposed borehole locations is a critical requirement prior to supply activation.

6. Conclusions

1. **High-Resolution Delineation:** Drone-borne magnetic tracking at a 10 Hz sampling interval successfully resolved three subsurface dolerite dykes, marked by distinct positive anomalies ranging from +198 to +949nT against the regional crystalline background.

2. **Structural Orientation Validated:** Magnetic gradient asymmetry values (G_s/G_n = 0.71-0.78) prove that the primary NW–SE dyke walls dip steeply northward (65-80^0). This orientation directly opposes the regional southward hydraulic flow, forming a natural underground dam system.

3. **Aquifer Geometry Quantified:** Peters' half-width transformations and depth sections map the unweathered basement floors at 75–134 m, identifying a primary fractured aquifer corridor up to 70 m thick along Profile L3.

4. **Development Recommendations:** Total exploitable groundwater volumes are calculated at 8.3 - 11.1 million litres. Eight target community boreholes are proposed on the upstream (northern) flanks of the dyke walls, alongside five surface check dams. Mandatory fluoride testing remains an essential requirement before supply deployment.

Acknowledgements

This investigation was executed pro bono for the Ekalavya Foundation as a voluntary humanitarian service to the Gond tribal communities of Komaram Bheem Asifabad district. The authors thank the Ekalavya Foundation for site data access and the local community members for field logistical cooperation. Central Ground Water Board reference data provided valuable hydrochemical baseline metrics. Data analysis, figure generation, and manuscript preparation were assisted by Perplexity Computer (Perplexity AI, San Francisco, CA, USA). No direct research funding was received for this project.

References

1. CGWB (2022). Aquifer Mapping and Management of Ground Water Resources – Kumuram Bheem Asifabad District, Telangana. *Central Ground Water Board*, Ministry of Jal Shakti, Government of India, Hyderabad.
2. Chalikakis, K., Plagnes, V., Guerin, R., Valois, R., and Bosch, F.P. (2011). Contribution of geophysical methods to karst-system exploration: an overview. *Hydrogeology Journal*, 19(6), 1169–1180.
3. Chand, R., Radhakrishna, I., Raju, D.C.V., and Subrahmanyam, V. (2004). Identification of structural lineaments using Landsat-7 ETM+ data and its correlation with seismicity in parts of Garo Hills, India. *International Journal of Remote Sensing*, 25(2), 433–439.
4. Chidichimo, F., De Biase, M., Rizzo, E., and Straface, S. (2014). Geophysical and hydrological data integration as support for hydrogeological conceptual model building. *Hydrology Research*, 45(6), 837–851.
5. Gustafson, G. & Kraskén, J. (1994). Prognosis for fracture groundwater flow with the σ-parameter. *Ground Water*, 32(3), 374–382.
6. Jackisch, R., Lorenz, S., Zimmermann, R., Mouli-Castillo, J., and Gloaguen, R. (2020). Drone- borne hyperspectral monitoring of acid mine drainage: An example from the Sokolov lignite district. *Remote Sensing*, 12(1), 123.
7. Krishnamurthy, J., Venkatesa Kumar, N., Jayaraman, V., and Manivel, M. (1996). An approach to demarcate groundwater potential zones through remote sensing and a geographical information system. *International Journal of Remote Sensing*, 17 (10), 1867–1884.
8. Nabighian, M.N. (1972). The analytic signal of two-dimensional magnetic bodies with polygonal cross-section: its properties and use for automated anomaly interpretation. *Geophysics*, 37(3), 507–517.
9. Parshin, A.V., Morozov, V.A., Blinov, A.V., Kosterev, A.N., and Budyak, A.E. (2018). Low-altitude geophysical magnetic prospecting based on multirotor UAV as a promising replacement for traditional ground survey. *Geo-spatial Information Science*, 21 (1), 67–74.

10. Peters, L.J. (1949). The direct approach to magnetic interpretation and its practical application. *Geophysics*, 14(3), 290–320.
11. Reynolds, J.M. (2011). *An Introduction to Applied and Environmental Geophysics* (2nd Ed.). Wiley-Blackwell, Chichester.
12. Telford, W.M., Geldart, L.P., and Sheriff, R.E. (1990). *Applied Geophysics* (2nd Ed.). Cambridge University Press, Cambridge.
13. Walter, C., Braun, A., and Fotopoulos, G. (2019). Impact of three-dimensional attitude variations of an unmanned aerial vehicle magnetometry system on magnetic data quality. *Geophysical Prospecting*, 67(2), 465–479.
14. Wenzel, W.W. and Blum, W.E.H. (1992). Fluoride speciation and its relevance for plant uptake and phytotoxicity. *Plant and Soil*, 139 (1), 35–44.
15. WHO (2022). *Guidelines for Drinking-Water Quality* (4th Ed., incorporating 1st addendum). World Health Organization, Geneva.